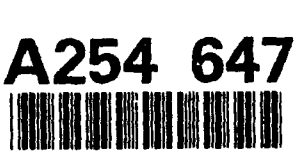

TECHNICAL REPORT BRL-TR-3393

BRL

COMPUTER-AIDED ANALYSIS OF FLASH X-RAY FILMS

RICHARD L. SUMMERS
KIPP C. WRIGHT

SEPTEMBER 1992

U.S. ARMY LABORATORY COMMAND

BALLISTIC RESEARCH LABORATORY
ABERDEEN PROVING GROUND, MARYLAND

NOTICES

Destroy this report when it is no longer needed. DO NOT return it to the originator.

Additional copies of this report may be obtained from the National Technical Information Service, U.S. Department of Commerce, 5285 Port Royal Road, Springfield, VA 22161.

The findings of this report are not to be construed as an official Department of the Army position, unless so designated by other authorized documents.

The use of trade names or manufacturers' names in this report does not constitute indorsement of any commercial product.

REPORT DOCUMENTATION PAGE

Form Approved
OMB No. 0704-0188

1. AGENCY USE ONLY *(Leave blank)*	2. REPORT DATE	3. REPORT TYPE AND DATES COVERED
	September 1992	Final, June 1990–June 1992

4. TITLE AND SUBTITLE
Computer-Aided Analysis of Flash X-ray Films

5. FUNDING NUMBERS
PR: 1L162618AH80

6. AUTHOR(S)
Richard L. Summers and Kipp C. Wright

7. PERFORMING ORGANIZATION NAME(S) AND ADDRESS(ES)
U.S. Army Ballistic Research Laboratory
ATTN: SLCBR-TB-W
Aberdeen Proving Ground, MD 21005-5066

8. PERFORMING ORGANIZATION REPORT NUMBER

9. SPONSORING / MONITORING AGENCY NAME(S) AND ADDRESS(ES)
U.S. Army Ballistic Research Laboratory
ATTN: SLCBR-DD-T
Aberdeen Proving Ground, MD 21005-5066

10. SPONSORING / MONITORING AGENCY REPORT NUMBER
BRL-TR-3393

11. SUPPLEMENTARY NOTES

12a. DISTRIBUTION / AVAILABILITY STATEMENT
Approved for public release; distribution is unlimited.

12b. DISTRIBUTION CODE

13. ABSTRACT *(Maximum 200 words)*

The shaped charge jet free-flight experiment is an extremely valuable diagnostic in the shaped charge design process. A semiautomated method is discussed for the digitization of a particulated jet's position and shape from the x-ray film image into electronic storage files, which provides the experimentalist with an efficient basis for data reduction. With the aid of a microcomputer, one can generate a wealth of information concerning the pertinent jet characteristics. Methods of computer-aided digitization of particulated jets and analysis of physical jet characteristics and performance are discussed.

14. SUBJECT TERMS
flash x-ray, flash radiography, shaped charges, jet characteristics, data reduction transverse velocity, drift velocity

15. NUMBER OF PAGES
42

16. PRICE CODE

17. SECURITY CLASSIFICATION OF REPORT	18. SECURITY CLASSIFICATION OF THIS PAGE	19. SECURITY CLASSIFICATION OF ABSTRACT	20. LIMITATION OF ABSTRACT
UNCLASSIFIED	UNCLASSIFIED	UNCLASSIFIED	UL

INTENTIONALLY LEFT BLANK.

TABLE OF CONTENTS

INTENTIONALLY LEFT BLANK.

LIST OF FIGURES

LIST OF TABLES

INTENTIONALLY LEFT BLANK.

1. INTRODUCTION

A cylinder of explosive with a hollow cavity in one end and a detonator at the opposite end is known as a shaped charge. The hollow cavity, which may assume almost any geometric shape is usually lined with a thin layer of metal. The liner, usually conical, forms a jet when the explosive charge is detonated. Upon initiation, a spherical wave propagates outward from the point of initiation. As the detonation wave engulfs the lined cavity, the material is accelerated under the high detonation pressure, collapsing the cone. The collapse of the material from a conical liner on the axis of symmetry forces a portion of the liner to flow in the form of a jet where the jet tip velocity can travel in excess of 10 km/s. Because of the presence of a velocity gradient, the jet will stretch until it fractures into a column of particles. This fracture of the jet into a series of particles is termed jet breakup or particulation.

The penetration of a shaped charge jet into most target materials increases to a maximum and then decreases as the standoff distance (the distance from the front of the shaped charge to the target) increases. This penetration peak occurs just prior to the onset of jet breakup. After particulation, the penetration decreases due to the dispersion, spread, and tumbling of the jet particles. A bowed jet or a particulated jet with substantial particle dispersion will not consistently strike the target at the same point. Therefore, the lack of jet straightness reduces the effective penetrating length of the jet. The straightness of a shaped charge jet can be quantified by the transverse velocity distribution in the jet.

The penetration process can be modeled with one-dimensional analytical codes or two- or three-dimensional hydrocodes. The one-dimensional models typically assume a hydrodynamic process since the pressures exerted at the jet-target interface greatly exceed the yield strength of the material. The one-dimensional models require jet characteristics (velocity, break-up time, virtual origin, etc.) derived from free-flight experiments as input.

In a free-flight experiment, the shaped charge jet is, typically, allowed to travel unimpeded through an air space which is 20 or more charge diameters (CD) in length. During the jet's transit through the air space, two to four flash radiographic images are obtained at predetermined time intervals. Flash radiography is necessary since ordinary photographs are uninformative due to obscurants associated with the detonation. The flash radiographs are

usually timed to allow the jet to particulate prior to the exposure time. Thus, several images of the particulated jet are captured on the film at known time intervals. The films are analyzed, and the collected data are reduced to yield the shaped charge jet characteristics. The data derived from the free flight can be utilized for three main purposes—for correlation with jet formation models; to predict the penetration as a function of standoff and target material; and to identify problems in the shaped charge manufacture and assembly.

Analysis of the flash radiographs of jet free flight is a time-consuming process demanding extremely high accuracy. In order to reduce analysis time and increase accuracy, a semiautomated procedure is used. This procedure involves the use of a manual digitizer table and a personal computer to convert pertinent film data to binary storage files, providing the experimentalist with an efficient basis for data reduction. Semiautomated film analysis procedures have been in use at the U.S. Army Ballistic Research Laboratory (BRL) and other institutions for quite some time (Blische and Simmons 1981; Segletes 1983, 1987; Fenton and Butz 1989; Summers, Walters, and Dick 1990). In addition, some researchers have begun to develop and use automated film analysis systems which use either a film scanner or camera to digitize the film in conjunction with software which measures the particle or fragment sizes and positions (Van Bree and Verhagen 1986; Verhagen and Van Bree 1987 and 1989; Lystad et al. 1989).

The automated procedures show great promise for increasing the measurement accuracy and for reducing the amount of tedium involved in radiographic analysis. A major obstacle to fully automated digitization of the jet free flight exists in the quality of the radiograph. Due to the large number of films involved in a single jet free flight, exposure of the film is not homogeneous over the entire length of the jet. Thus, the background and the jet particles are not evenly exposed over the entire film length. Inconsistencies in the background of the radiograph create a large problem for edge detection, and thus more work is required to fully automate the process.

Improvements in the speed and memory storage capabilities of minicomputers have brought about several improvements to the previous methods of semiautomated film analysis which were in use at the BRL. In the past, one was required to simulate a particle's shape using a limited number of points. For example, Blische and Simmons (1981) used six points

to simulate the particle as two truncated cones sharing the same cylindrical base. Fenton and Butz (1989) used a similar method but allowed only three points per particle. The three points simulated the particle as two abutted right circular cones. In both cases the accuracy is, to a large extent, dependent upon the digitizer operator's discretion in choosing which points best describe the particle's outline. The method currently in use, and described in this report, allows the digitizer operator to digitize up to 100 points per particle. Some discretion is still involved since, in most cases, less than 20 points per particle are digitized. The particle is plotted on the computer screen as the points are digitized to allow the operator to verify that an accurate representation of the particle geometry has been captured. Subsequently, all of the points which are digitized are stored for later analysis. The primary advantage of this method is that the raw data are available on a computer disk, and any assumptions needed to estimate a particle's mass, axis of symmetry, etc., can be modified or refined and recalculated without having to redigitize the films. As a result, the radiographic analysis is divided into three steps. First, the image is digitized, and the raw data are stored. Second, the digitized data are analyzed, and the characteristics of each individual particle are determined. Finally, the information is tabulated, and the overall jet characteristics are derived.

2. EXPERIMENTAL TECHNIQUES

The shaped charge liner is precisely aligned using both surveying equipment and a laser alignment device. A Cartesian coordinate system, shown in Figure 1, is defined with origin placed at the axis of symmetry of the charge and the base of the liner. The positive z-axis coincides with the intended shotline in the direction of jet travel. The positive y-axis points vertically upward, and the positive x-axis points toward the film, away from the flash x-ray sources.

The radiographs are digitized with a digitizer table which was manufactured by the GTCO Corporation of Rockville, MD. The films from a test firing are analyzed using a program which drives the digitizer and performs initial calculations based on the digitizer input and the test setup. The program is structured to read data obtained using up to four flash times. The input required to execute the digitizer program includes the range of particles to be analyzed for each flash time, the number of films which were used in the test, the magnification factors,

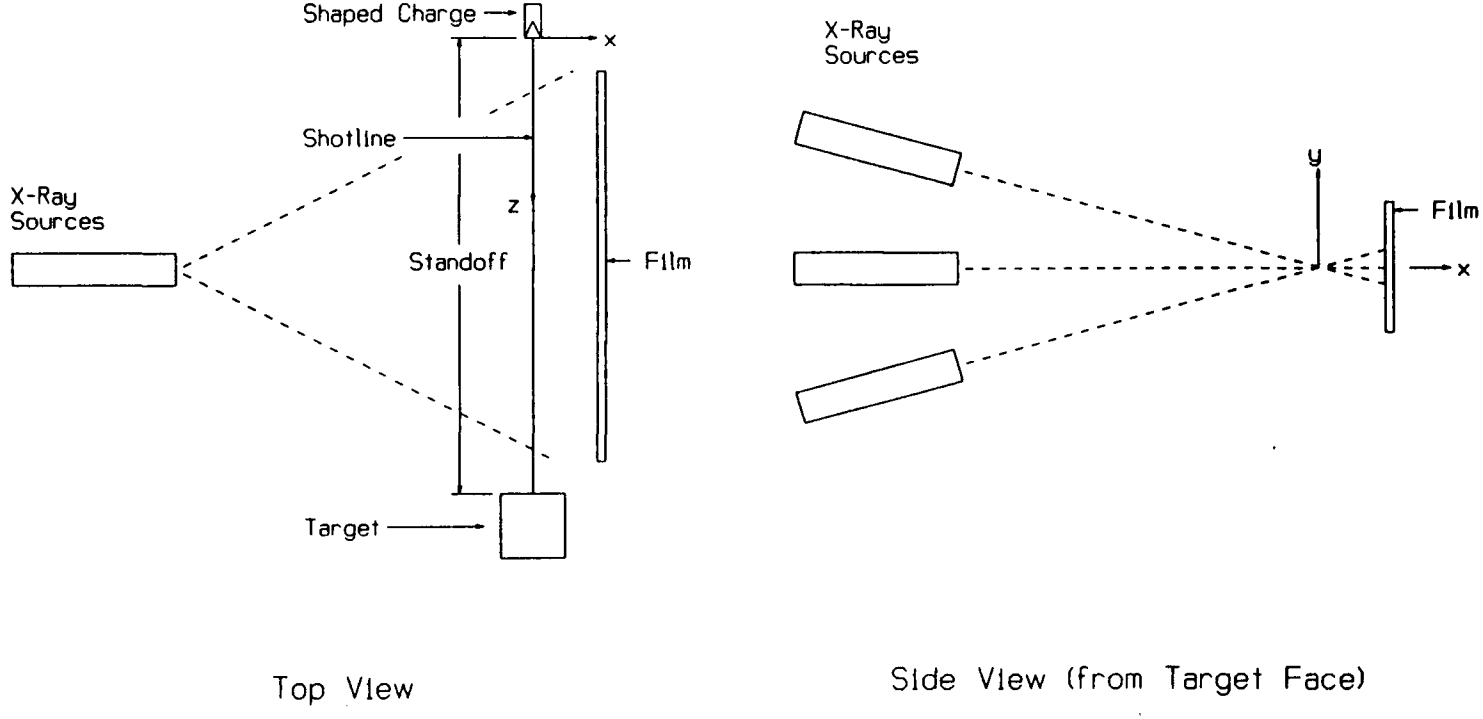

Figure 1. Test Site Configuration at ERF-16.

the fiducial locations on each film, the jet density, and the test setup parameters. Each particle that appears on the films is numbered starting at the tip of the jet. The images from an individual test which are produced at each flash time are compared with the images from other flash times to ensure that the same particle is designated with the same particle number in each flash. Initial calculations are performed which modify the image dimensions and location to reflect the magnification factor and to place the image in a known frame of reference. In addition, each digitized particle image is stored in a data file for further analysis. Figure 2 shows a portion of an x-ray film and the digitized representation of the jet particle images.

2.1 Analysis. After the jet particles have been digitized, a program which determines the characteristics of the individual particles is executed. The first calculation performed is to obtain the individual particle positions at each flash time. The particle position is defined as the position of the particle's center of mass. The center of mass is determined under the assumption that the projection of the jet particle into and out of the plane of the film is symmetric. Integrating over the contour of a particle, one can calculate the x and y moments of inertia of the particle in the plane of the film. The digitizing process simulates each particle's contour discretely so these moments are defined for the areas between each digitized point and the axis of symmetry of the warhead or shotline (Figure 3). The area between the particle and the shotline is negated when the summation is taken over all of the areas, leaving only the particle's cross-sectional area to contribute to the moment and area calculations. The resultant x and y moments of inertia are divided by the cross-sectional area to give the x and y coordinates of the center of mass.

The placement of the axis of symmetry of a particle requires user interaction. The program chooses as a first approximation the line connecting the two points on the contour of a particle farthest from one another. This line is chosen as a default because most ductile jet particles tend to neck and eventually break along the jet's axis of symmetry. The user may choose the default or may choose a new axis which appears to bisect the particle more evenly. The location of the axis of symmetry is critical because it is used to derive other particle characteristics such as length, radius, and mass. The length of a particle is given as both the length along the axis of symmetry and as the distance between the two points on the boundary which are the farthest apart. The maximum radius is defined as the greatest normal

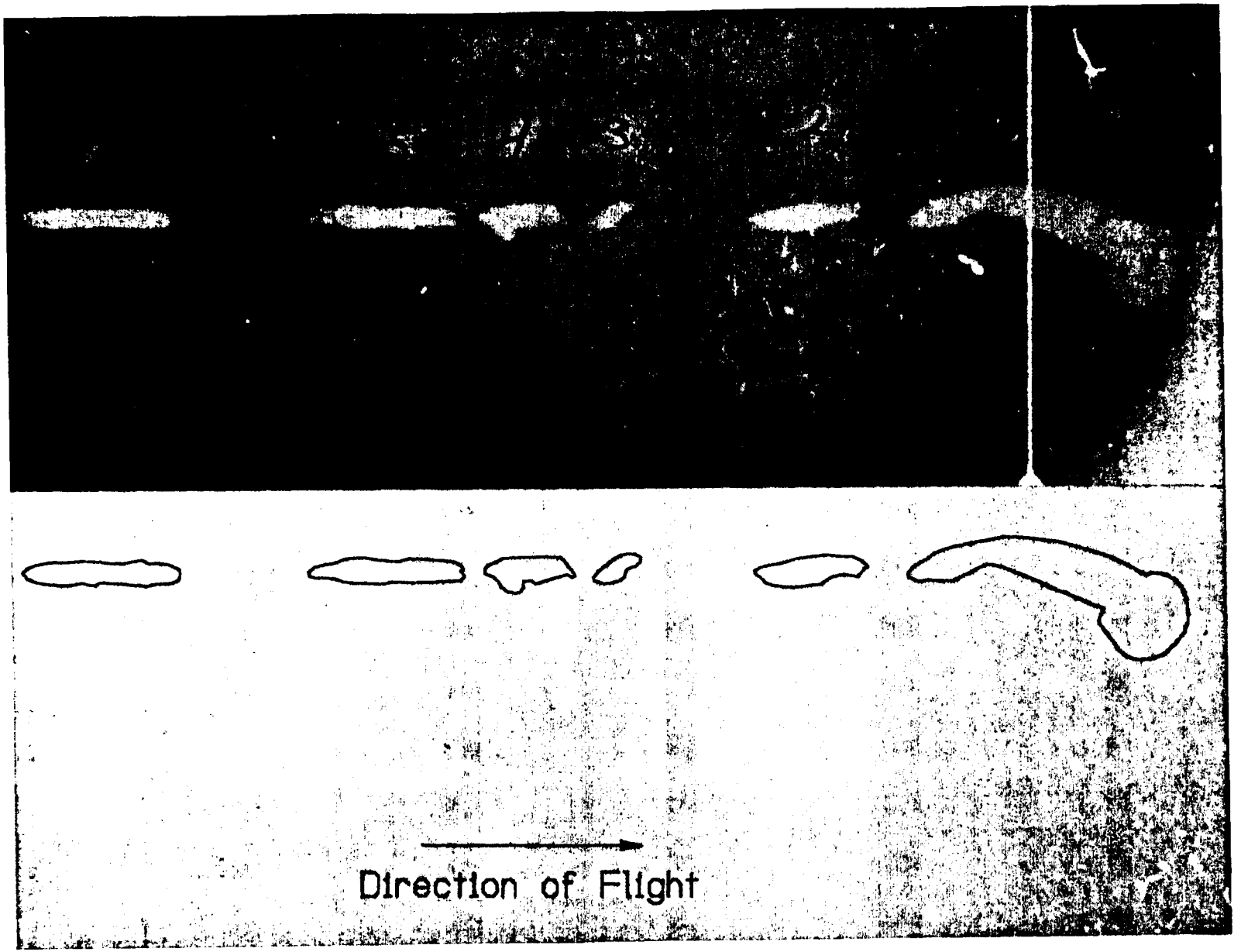

Figure 2. Comparison of an Actual Radiograph to the Digital Representation.

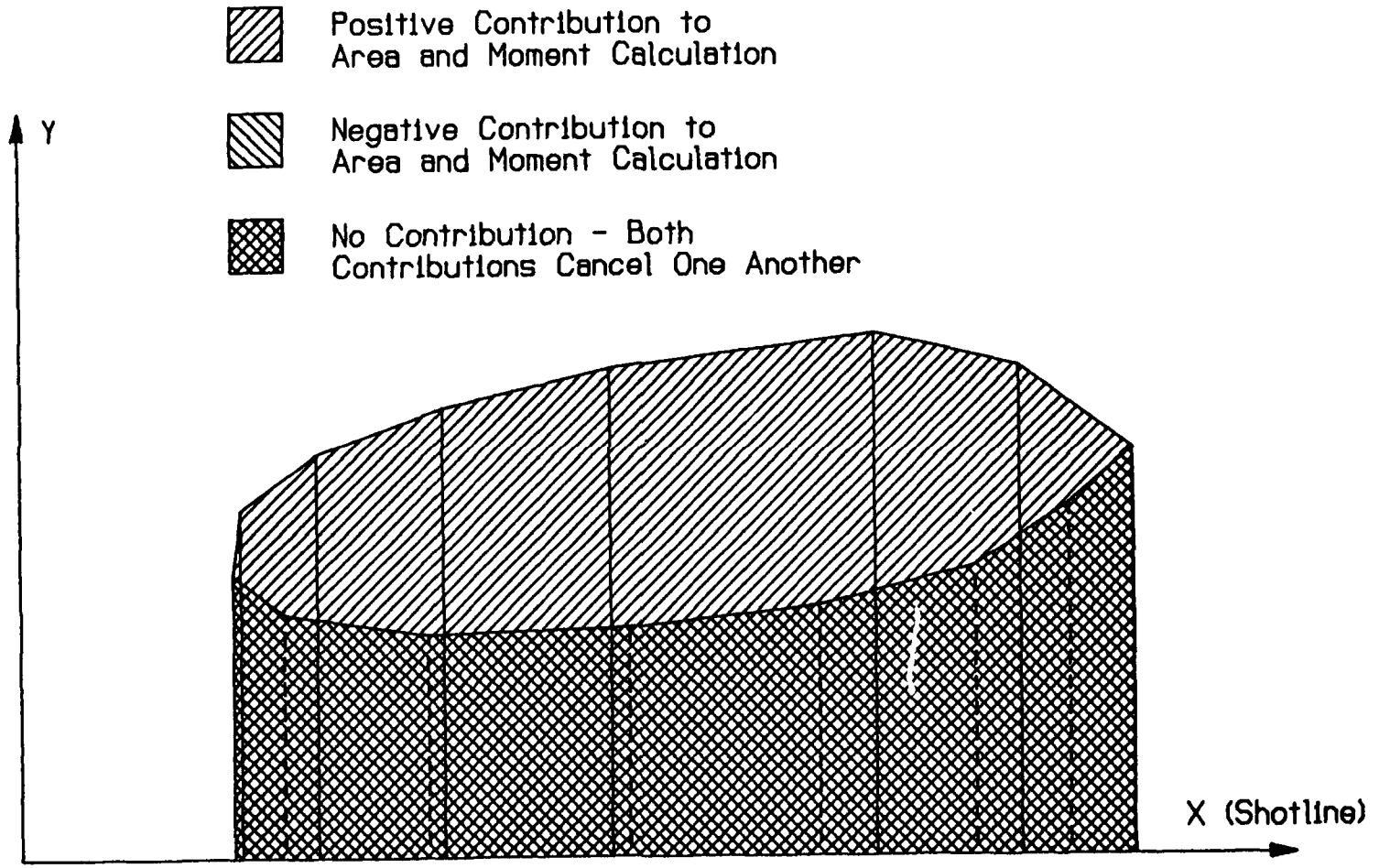

Figure 3. Regions of Contribution to the x and y Moments of Inertia Calculation.

distance between any point on the particle boundary and the axis of symmetry. The volume is calculated assuming that each section between two digitized points and the axis of symmetry is half of a truncated cone. Figure 4 shows how a section is defined. The particle volume is the summation of these sectional volumes. The mass is obtained by multiplying particle volume by the virgin jet density.

The third step in the digitization process is to pool all the above information, tabulate the data, and calculate axial and transverse velocities, jet breakup times, the virtual origin, the formation time, cumulative values of jet length, mass, momentum, and kinetic energy, and the average particle characteristics. The transverse velocity of a particle is defined as the velocity of the particle in a direction perpendicular to the axis of symmetry of the shaped charge liner. The jet breakup times, the virtual origin, and the formation time are idealized values which are used as inputs for analytical penetration models. The breakup time is calculated as the total jet length divided by the axial velocity difference between the tip and the tail of the jet, as suggested by Simon (1974). The virtual origin is defined as the point from which the jet emanates. The formation time is the time at which the jet emanated from the virtual origin. Both the virtual origin and the jet formation time are calculated by performing a linear regression analysis of the particle position vs. velocity (Blische and Simmons 1981). It should be emphasized that the breakup time, virtual origin, and formation time are all idealized values and may vary significantly depending on the number of jet particles included in the analysis.

2.2 Velocity Calculations. Both the axial and transverse velocity of a particle are determined using the location of the center of mass of a particle. The axial velocity is calculated as described by Blische and Simmons (1981) and Summers, Walters, and Dick (1990). If more than two flash x-ray exposure times are available, an average axial velocity is calculated for each particle. For example, if three flash times are used, the particle velocities are calculated between the first and second flash times, the first and third flash times, and the second and third flash times. This repetitive measurement of jet particle velocity can reveal errors in the test setup or in the digitization process.

The transverse velocity of a jet particle is defined as the velocity of the jet particle in a direction perpendicular to the axis of symmetry of the shaped charge. The measurement of

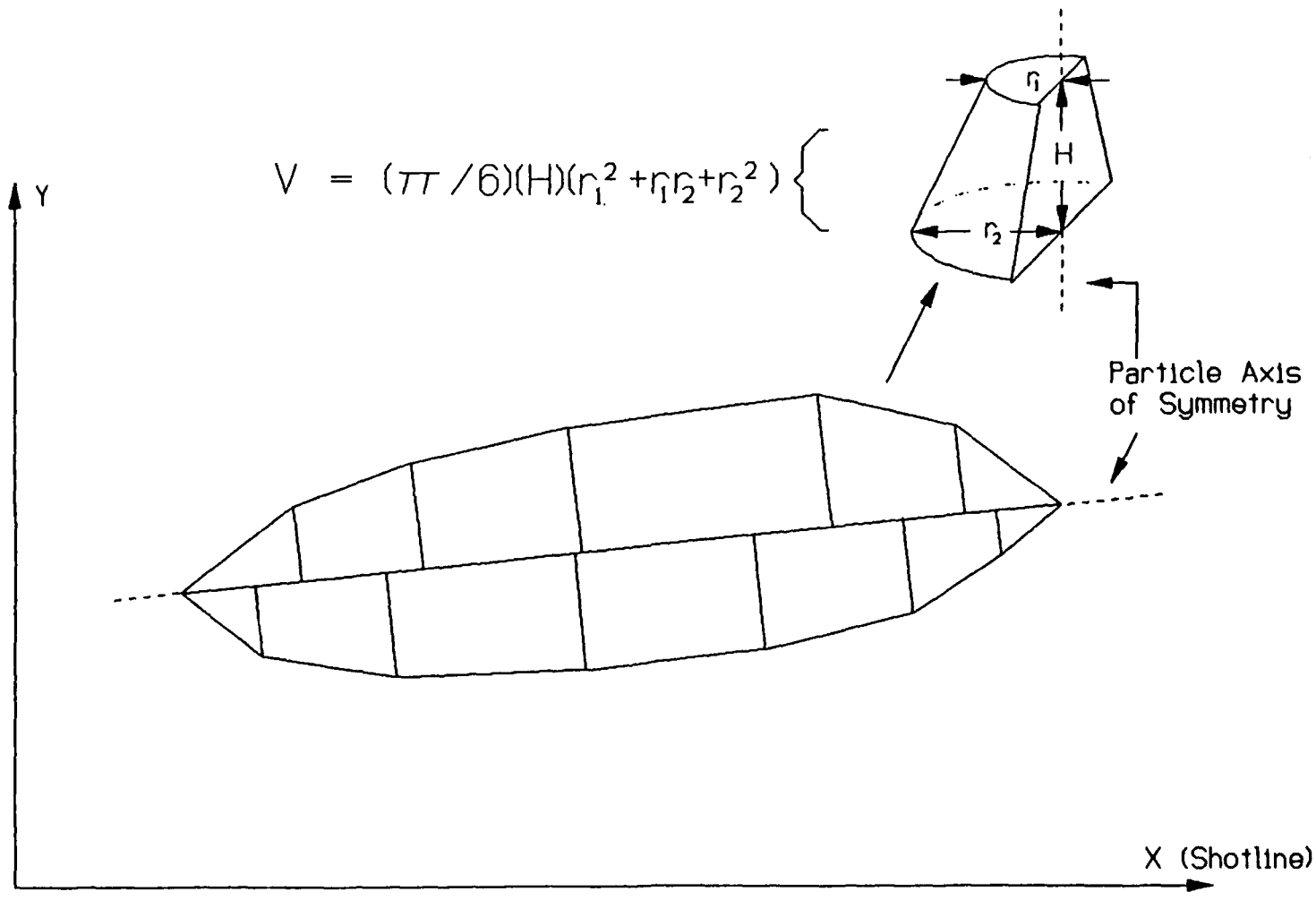

Figure 4. Volume Calculation by Summation of Segmented Regions.

transverse velocity is particularly difficult due to the extreme level of accuracy required. For example, consider a shaped charge particle with an axial velocity component of 5 km/s and a transverse velocity component of 25 m/s. If the time interval between flash x-ray pulses is 100 μs, then a measurement error of 1 mm results in an accuracy of ± 0.2% for the axial velocity and ± 40% for the transverse velocity. In addition, if the charge axis is tilted by as little as 1° from the intended shotline, then a jet particle with an axial velocity component of 5 km/s will appear to have a transverse velocity in excess of 85 m/s. Thus, great care must be taken in the experimental procedure and the interpretation of the resulting data.

The measurement of the transverse velocity of a jet particle has been accomplished using both streak cameras and flash x-rays. Measurement techniques have been discussed by Held and Nikowitsch (1984), Segletes (1983; 1987), and Sewell (1989) among others. Held describes the use of both orthogonal synchronized streak cameras and flash x-rays to measure jet transverse velocities. Segletes and Sewell both discuss measurement techniques involving flash x-ray equipment. Sewell recommends the use of highly accurate surveying equipment to ensure the proper alignment of the shaped charge; thus, reducing the possibility of any alignment errors during the experiment.

If two or more sets of simultaneous orthogonal flash x-rays are available, then the transverse velocity can be measured directly. However, as a matter of economics and practicality, this flash x-ray source arrangement is not always feasible due to site versatility, site expense, and amount of film coverage. The transverse velocity is calculated using techniques developed by Segletes (1987) and Summers and Wright (1992), which do not require multiple sets of simultaneous orthogonal flash x-rays. Segletes' method operates under the assumption that the transverse velocity of a jet particle is constant and is imparted to the jet particle at the theoretical point in time and space from which the jet emanates (known as the virtual origin). However, the virtual origin is a theoretical idealization of the actual data. In addition, Held (1989) has shown that the transverse velocity of a portion of a shaped charge jet can be significantly increased by the particulation process. Thus, an extension to Segletes' method has been derived which allows the determination of transverse velocity with the single assumption that the transverse velocity is constant after the jet has particulated.

The digitized data provides the projection of the jet in the y-z plane. Only the vertical separation, D, between the shotline and each particle is measured directly. If the event is observed in the normal (x-y) plane, the actual distance between the shotline and each particle, L, can be derived as shown in Figure 5. The distance L is, thus, defined by the equation

$$L = \frac{D}{\left(\sin\theta - \frac{\cos\theta}{\tan\gamma}\right)} .$$

Using two different flash radiographs of the free flight, the transverse velocity is calculated as the change in the distance L between flashes divided by time difference between exposures, i.e.,

$$V_T = \frac{L_2 - L_1}{t_2 - t_1} ,$$

where t is the time at which the films were exposed and the subscripts refer to the exposure number. If three nonsimultaneous exposures are available, then by equating the transverse velocity equation between two different flash combinations, an expression involving tan θ is developed. Thus, if

$$\frac{L_2 - L_1}{t_2 - t_1} = \frac{L_3 - L_1}{t_3 - t_1} ,$$

then it can be shown that

$$A \tan^2\theta + B \tan\theta + C = 0 ,$$

where

$$A = (D_2 - D_1)T - (D_3 - D_1) ,$$

$$B = (D_1g_2 + D_1g_3 - D_2g_1 - D_2g_3)T - (D_1g_2 + D_1g_3 - D_3g_1 - D_3g_2) ,$$

$$C = (D_2g_1g_3 - D_1g_2g_3)T - (D_3g_1g_2 - D_1g_2g_3) ,$$

$$T = \frac{(t_3 - t_1)}{(t_2 - t_1)} , \text{ and}$$

$$g_i = \cot\gamma_i .$$

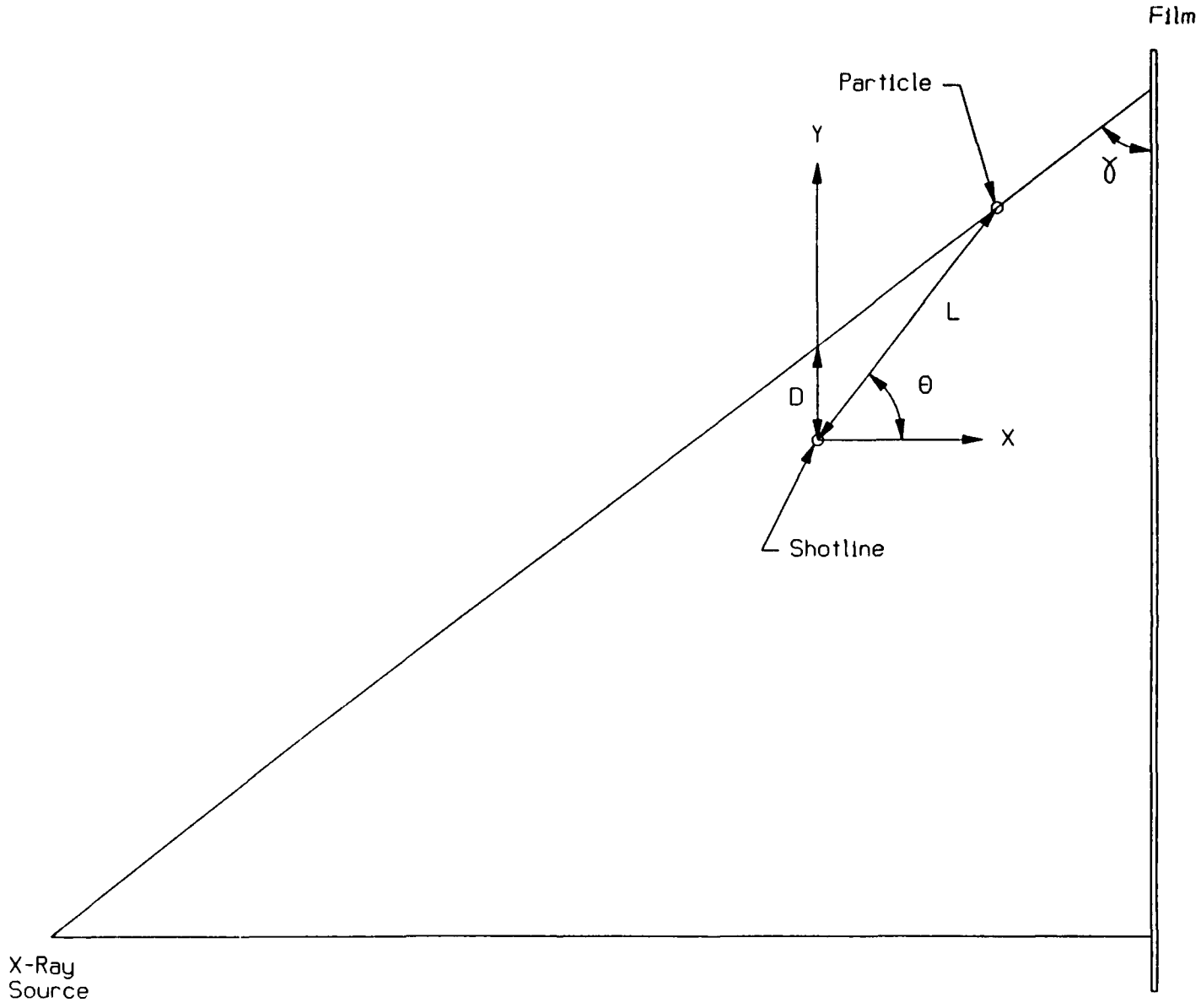

Figure 5. Coordinate System Used for Transverse Velocity Calculations.

The quadratic equation is used to solve for the two roots of tan θ. In most cases, the correct value of θ can be determined from the impacts on the target plate. For example, one value of θ will yield a transverse velocity on the order of 1,000 m/s, which can clearly be discarded if the target plate shows little deviation from the intended impact point. However, two problems can arise. In some cases, the discriminate in the quadratic is negative, yielding an imaginary value for θ. Such cases are either a result of the error involved in the measurement process, or they are due to the assumption of constant transverse velocity. In addition, it is possible to arrive at two realistic values of θ. Cases have arisen in which the two roots of tan θ resulted in values of transverse velocity which were similar in both magnitude and direction. Methods which may eliminate these problems are currently being evaluated. One possible method is to provide one set of simultaneous, orthogonal flash x-ray exposures in conjunction with two nonsimultaneous exposures. The simultaneous exposures allow a direct measurement of the particle position at some point in time, thus providing a reference position and the direction of the transverse motion for each particle. Under the assumption that the direction of travel is constant, the magnitude of the transverse velocity is derived explicitly.

Despite the accuracy involved in placing the shaped charge and its shotline, tilt is still a concern. A slight warhead tilt can result in large transverse velocity measurements. A perfectly aligned jet which is tilted will possess a transverse velocity distribution with the greatest transverse velocity at the jet tip and the lowest transverse velocity at the tail of the jet. However, the angle between the intended shotline and each jet particle (termed the dispersion angle) would be constant. The transverse velocity derived above is measured with respect to the predetermined shotline of the test configuration. To account for any possible tilt, a new shotline is derived from the data above (Segletes 1987). The x and y components of the dispersion angle are determined for each particle. For example, the tangent of the x component of the dispersion angle is defined as the x component of the transverse velocity divided by the axial velocity of the particle. The mean components of the dispersion angle provide an estimate of the warhead tilt in both the x and y directions. Once found, the transverse velocities relative to the original shotline are recomputed to account for the estimated warhead tilt. The end result is referred to as the absolute transverse velocity. In this manner, a perfectly aligned, but tilted, jet will possess zero absolute transverse velocity.

3. SAMPLE RESULTS

The data acquired from a free flight of a 140-mm shaped charge with a conical copper liner has been included. The experiment, Round 4264, was performed at the BRL Experimental Research Facility 16 by C. V. Paxton and J. W. Gardiner. A digital reproduction of this jet is illustrated in Figure 6. The data generated from the x-ray film analysis can be easily accessed to plot jet characteristics and trends.

Table 1 lists the distance from the base of the shaped charge liner to the center of mass of each particle at each flash time. Particle number 10 was obscured in flash 2 and was not digitized. Tables 2–5 give the length along the particle's axis of symmetry, the maximum length of each particle, the maximum radius of each particle, and the mass of each particle at each flash time. The jet tip particle (particle number 1) is bending, and, therefore, the length of the particle's image on the film is dependent on the angle at which the particle is viewed. This results in large discrepancies in the measured dimensions of the particle at different flash times. Table 6 provides the average length (along the particle axis of symmetry), radius, mass, length-to-diameter ratio, and axial velocity for each jet particle. Finally, Table 7 gives the cumulative properties of the jet. The breakup time, reported in Table 7, varies with the number of jet particles included in the calculation but approaches a constant value as the number of digitized particles is increased.

A wide variety of data can be generated from the digitizing process. Figure 7 is a plot of the axial velocity vs. each jet particle's axial position at each flash time. A linear regression analysis performed on each of the data sets shown in Figure 7 provides the virtual origin (the x intercept). The virtual origin is measured with respect to the base of the shaped charge liner and is positive in the direction of jet flight. In this case, the virtual origin was determined to be –49 mm from the base of the liner. Figure 8 is a plot of the axial jet velocity vs. the cumulative length. The negative of the slope of this curve is the breakup time. The plot shown in Figure 8 is useful in determining the validity of the breakup time approximation. Ideally, a plot of jet velocity vs. cumulative length should result in a straight line. If a good linear relation is not evident, then the curve may be treated as piecewise linear (Held 1985) to determine separate breakup times for several velocity ranges.

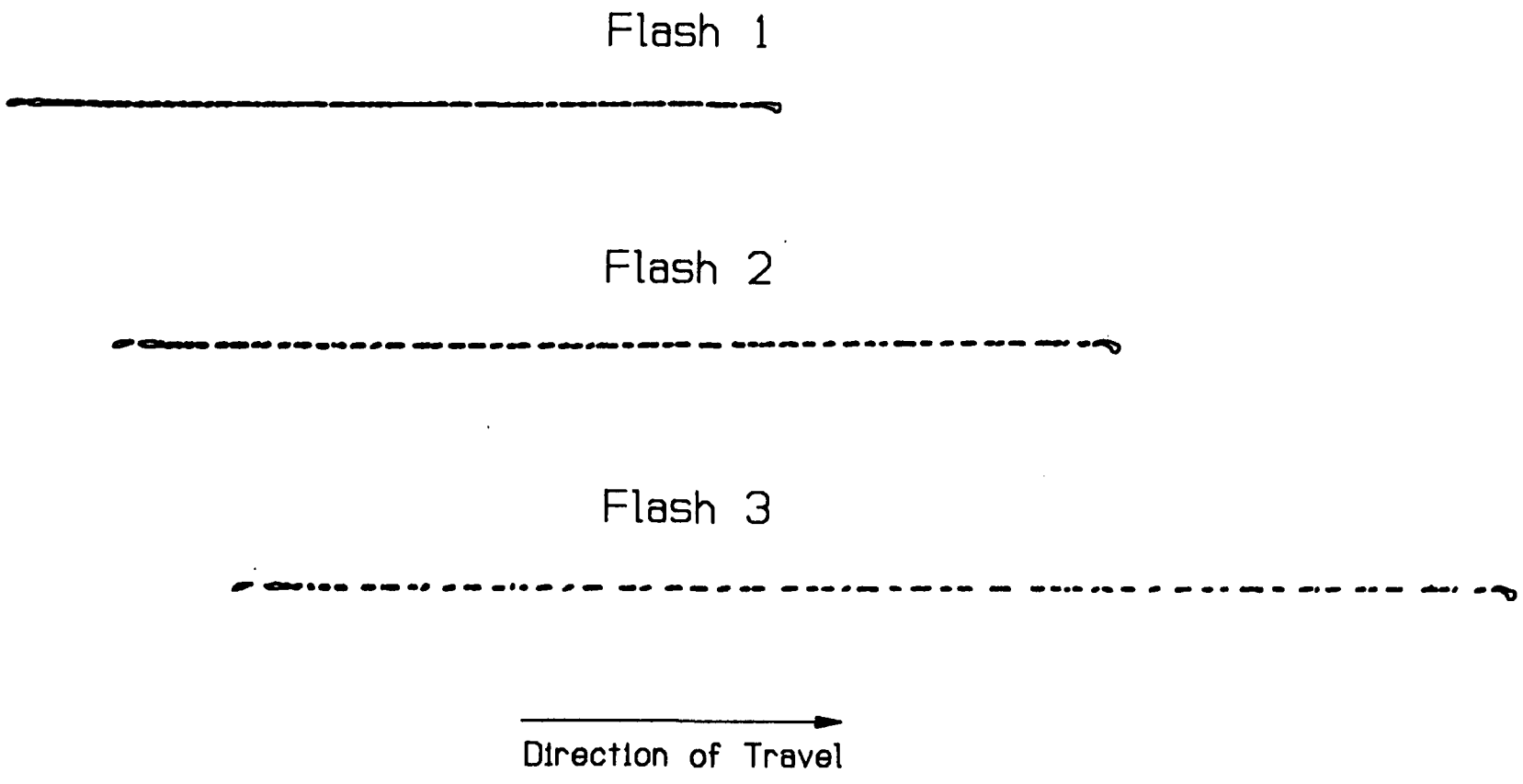

Figure 6. Digital Reproduction of the Radiographs Obtained From Round 4264.

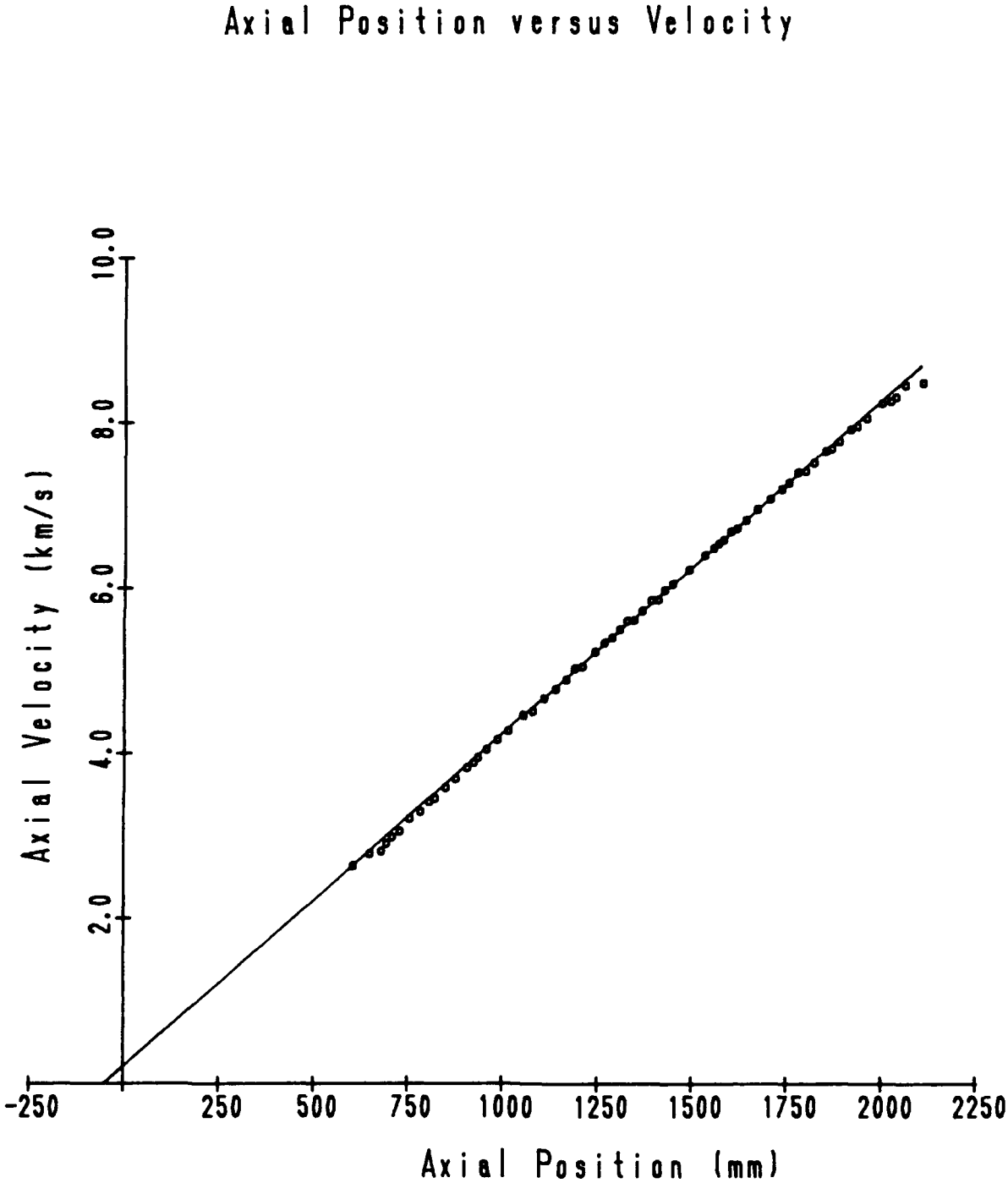

Figure 7. Plot of Axial Position vs. Axial Velocity.

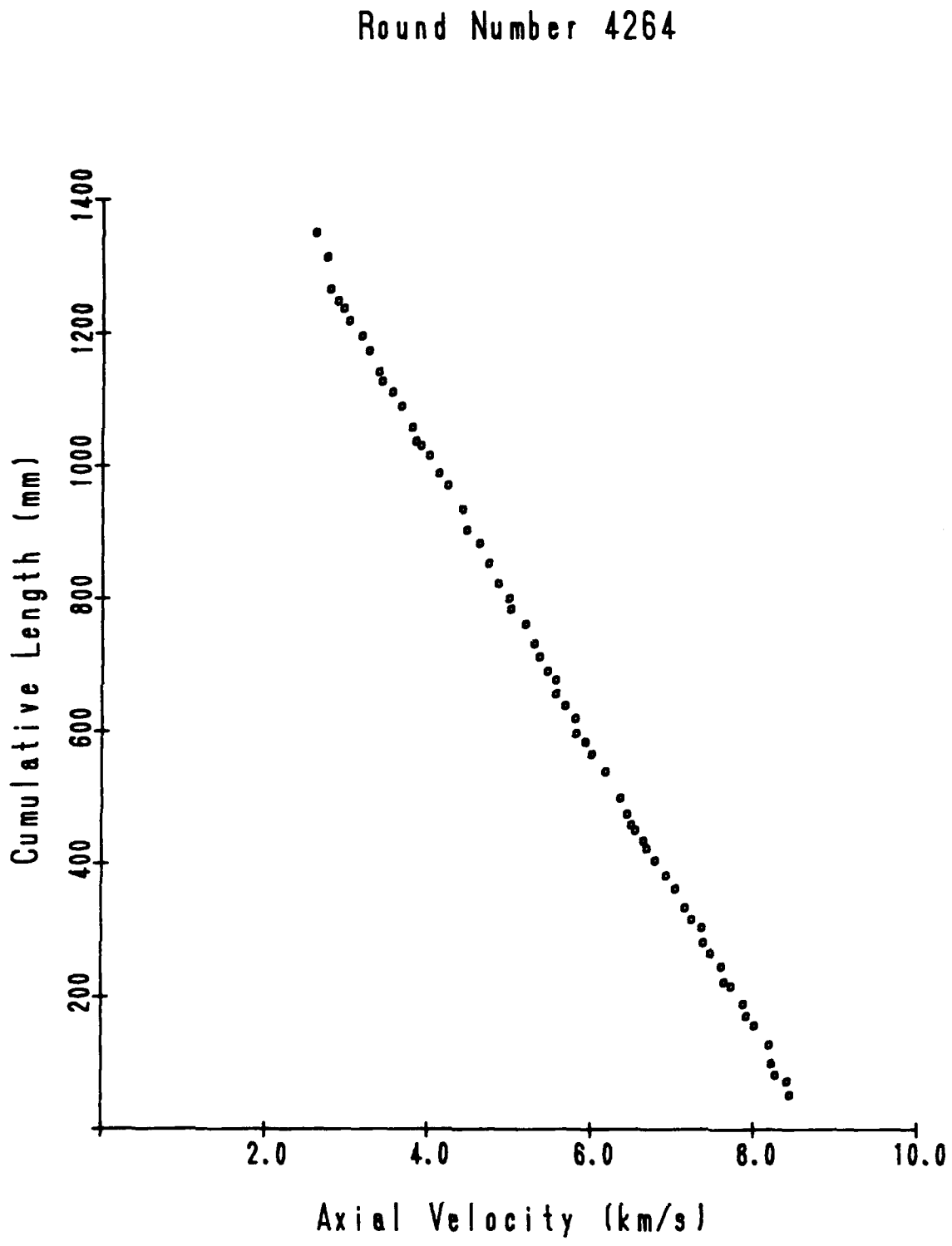

Figure 8. Plot of Axial Velocity vs. Cumulative Jet Length.

The measurement of the transverse velocity of each jet particle enables one to plot the location where each of the jet particles will strike the target plate. Such a plot provides information on the accuracy of the transverse velocity measurement and on which regions of the jet were badly misaligned. Figure 9 is a picture of the front of a target plate which was penetrated by a copper shaped charge jet. The cross on the target plate indicates the position of the intended shotline. Superimposed on Figure 9 is a plot of the expected impact points of the center of mass of each of the jet particles which were characterized.

The distance from the base of the shaped charge liner to the target plate in this experiment was 5,308 mm (38 charge diameters). The data indicates that the slower moving jet particles, travelling at a velocity less than 3.2 km/s, either struck the crater wall or the target face and did not add to the depth of penetration. This is not unexpected due to the very large standoff distance and because slower jet particles require greater time to reach the target and are, therefore, more greatly affected by transverse velocities.

A good agreement is achieved in both the location of the impacts on the target plate and the direction in which the target plate is slotted. The transverse velocity measured for each jet particle is given in Table 8. The warhead, as measured from the transverse velocity calculations, was tilted 0.12° in the x direction and 0.09° in the y direction. An estimate of the center of the hole in the target plate provides an x-tilt angle of 0.22° and y-tilt angle of 0.05°. The primary crater on the target plate is approximately 110 mm in diameter. The greatest distance between the predicted impact points is 43 mm. The hole in the target plate is larger than that plotted for two reasons. First, the plot only shows the location of target impact and does not account for the orientation of the jet particle or for hole growth due to high velocity impact phenomena. Second, due to the velocity gradient in a shaped charge jet and the limited amount of x-ray film coverage available, not every particle in the jet is characterized. The plot shown in Figure 9 covers the first 62 jet particles. The axial velocity of the slowest jet particle measured was 2.6 km/s. An additional 10 to 20 particles also impacted the target plate but were not characterized due to lack of film coverage.

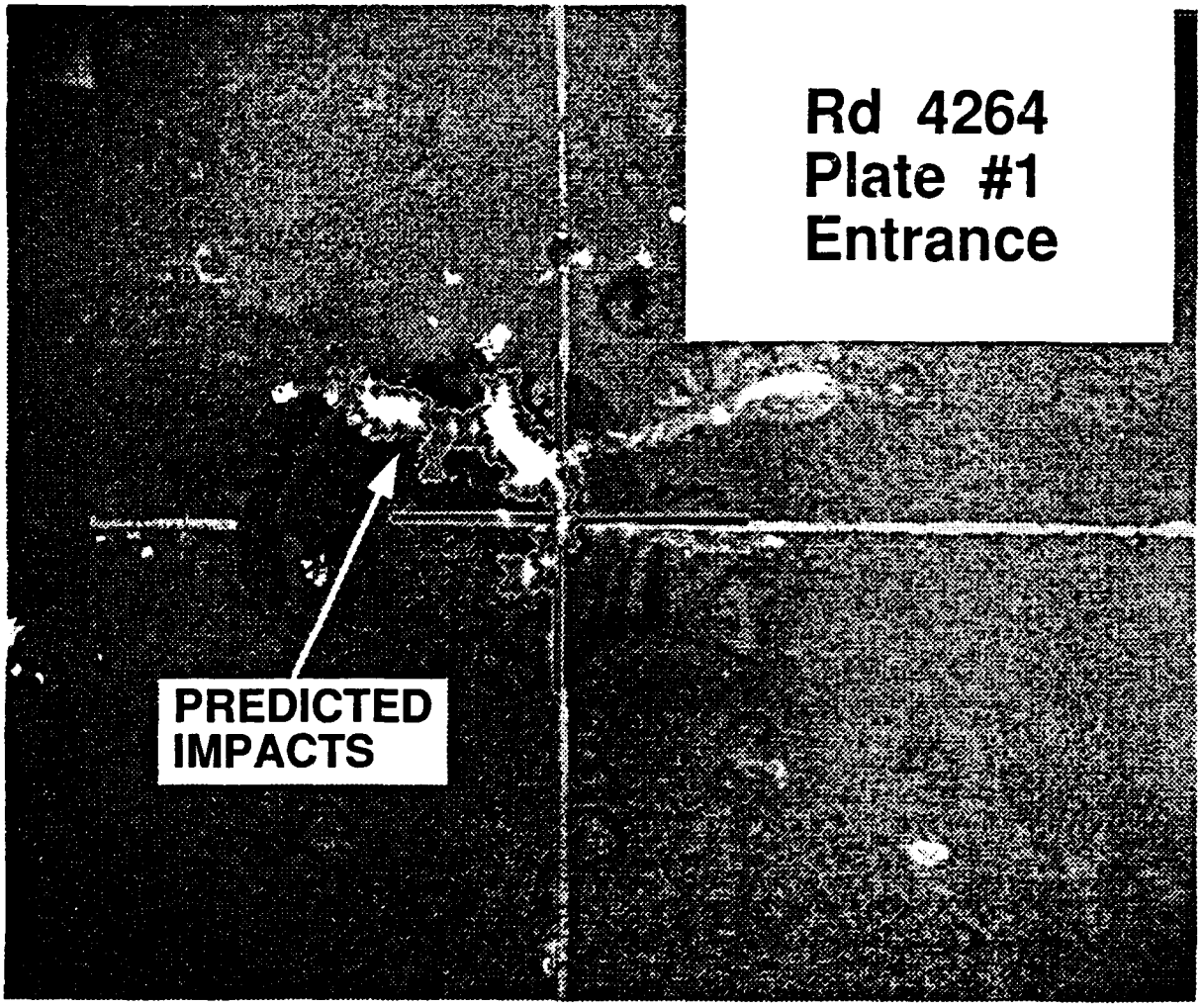

Figure 9. Predicted Jet Impacts Superimposed on the Actual Target Plate.

4. SUMMARY

The goal of this digitization and analysis process is to provide the experimentalist with as much pertinent information as is possible from radiographs of the jet free flight. There are several advantages of the data reduction algorithms discussed in this report. The programs were designed to provide quick feedback in the form of both tabular and graphical data. The raw data are stored to allow a complete digital reconstruction of the flash radiographs, which enables the researcher to perform additional case-dependent analyses. The mass, location, and dimensions of the particles are more accurately defined than in previous digitization methods. Finally, an improved method of calculating transverse velocities is utilized.

Though fully automated digitization is not used at this time, the programs were designed to accept this capability. In the future, to reduce time and tedium and also increase the accuracy of the data collected, the process should be updated to provide automated digitization. At the moment, there are many systems on the market which can automatically scan and digitize a radiograph. However, edge detection algorithms which find and define the contour of a particle are still not fully adequate or automatic.

Table 1. Standoff Distances Measured From the Liner Base

Particle	Flash No. 1 t = 295.0 (mm)	Flash No. 2 t = 375.0 (mm)	Flash No. 3 t = 470.0 (mm)
1	2,104	2,787	3,585
2	2,056	2,735	3,532
3	2,031	2,699	3,481
4	2,017	2,682	3,461
5	1,994	2,655	3,431
6	1,953	2,601	3,359
7	1,928	2,567	3,317
8	1,911	2,547	3,292
9	1,880	2,504	3,235
10	1,861	—	3,204
11	1,846	2,461	3,183
12	1,815	2,420	3,127
13	1,793	2,390	3,088
14	1,773	2,368	3,064
15	1,750	2,335	3,020
16	1,730	2,309	2,986
17	1,700	2,271	2,937
18	1,667	2,226	2,880
19	1,637	2,186	2,827
20	1,612	2,154	2,786
21	1,596	2,134	2,762
22	1,577	2,107	2,725
23	1,564	2,091	2,705
24	1,550	2,073	2,682
25	1,527	2,044	2,645
26	1,485	1,988	2,571
27	1,443	1,932	2,499
28	1,420	1,903	2,463
29	1,403	1,876	2,425
30	1,385	1,858	2,407
31	1,361	1,825	2,362
32	1,340	1,793	2,318
33	1,321	1,773	2,298
34	1,304	1,749	2,264
35	1,284	1,721	2,228
36	1,263	1,696	2,196

Table 1. Standoff Distances Measured From the Liner Base (continued)

Particle	Flash No. 1 t = 295.0 (mm)	Flash No. 2 t = 375.0 (mm)	Flash No. 3 t = 470.0 (mm)
37	1,237	1,660	2,151
38	1,204	1,613	2,087
39	1,184	1,591	2,061
40	1,162	1,559	2,018
41	1,134	1,521	1,969
42	1,103	1,481	1,918
43	1,074	1,440	1,863
44	1,050	1,411	1,828
45	1,010	1,357	1,757
46	981	1,319	1,708
47	953	1,283	1,659
48	928	1,251	1,618
49	917	1,235	1,596
50	901	1,213	1,568
51	871	1,173	1,516
52	842	1,135	1,469
53	817	1,100	1,420
54	800	1,079	1,396
55	776	1,046	1,352
56	749	1,011	1,308
57	721	971	1,253
58	700	945	1,221
59	686	924	1,194
60	673	905	1,165
61	642	870	1,128
62	596	812	1,055

Table 2. Jet Particle Lengths Measured Along Each Particle's Axis of Symmetry

Particle	Flash No. 1 t = 295.0 (mm)	Flash No. 2 t = 375.0 (mm)	Flash No. 3 t = 470.0 (mm)
1	56.1	53.5	48.5
2	20.2	21.1	20.9
3	9.6	9.9	9.2
4	16.5	15.4	16.4
5	28.4	29.1	28.4
6	29.1	29.7	30.1
7	14.6	14.6	14.4
8	17.7	16.9	17.4
9	26.2	26.5	25.9
10	7.5	—	6.2
11	23.6	22.9	24.1
12	20.0	19.4	19.2
13	15.0	16.1	16.6
14	22.3	22.6	22.9
15	12.0	12.2	11.6
16	17.8	17.5	18.2
17	29.0	27.7	28.4
18	19.5	20.1	20.1
19	23.4	22.6	22.2
20	18.7	17.9	17.5
21	12.5	12.2	11.3
22	15.4	15.5	15.8
23	8.8	7.6	9.3
24	16.5	16.2	16.5
25	25.5	23.5	23.5
26	41.2	40.6	37.8
27	25.6	26.1	26.4
28	17.9	18.0	17.8
29	13.1	13.4	13.6
30	23.5	23.5	23.2
31	18.5	18.7	17.8
32	18.2	17.8	18.0
33	19.8	21.5	21.3
34	13.6	13.0	13.9
35	21.5	21.7	22.1
36	19.8	18.6	19.4

Table 2. Jet Particle Lengths Measured Along Each Particle's Axis of Symmetry (continued)

Particle	Flash No. 1 t = 295.0 (mm)	Flash No. 2 t = 375.0 (mm)	Flash No. 3 t = 470.0 (mm)
37	29.0	29.0	29.7
38	23.9	23.2	22.8
39	16.2	15.4	16.2
40	22.7	22.0	23.2
41	30.2	30.2	31.3
42	30.0	30.4	30.4
43	19.1	19.8	19.8
44	30.5	31.7	30.8
45	36.0	35.9	35.6
46	18.7	17.6	19.1
47	26.3	26.1	26.4
48	14.1	15.7	12.3
49	6.9	5.3	7.3
50	22.3	21.7	21.1
51	31.4	32.0	31.0
52	21.1	20.4	20.8
53	18.8	15.9	16.1
54	14.0	13.9	14.5
55	30.1	33.3	33.3
56	22.2	23.4	24.4
57	22.4	22.0	22.3
58	18.6	18.9	19.2
59	10.0	12.2	11.1
60	17.0	17.3	18.9
61	44.8	49.5	48.7
62	37.5	38.1	36.5

Table 3. Maximum Jet Particle Lengths

Particle	Flash No. 1 t = 295.0 (mm)	Flash No. 2 t = 375.0 (mm)	Flash No. 3 t = 470.0 (mm)
1	56.2	53.5	48.7
2	20.8	21.5	20.9
3	9.6	9.9	9.2
4	17.0	17.2	17.3
5	29.8	29.6	29.2
6	29.1	29.7	30.1
7	14.6	14.6	14.4
8	17.7	17.3	17.4
9	26.2	27.5	26.8
10	7.5	—	6.2
11	24.9	22.9	25.1
12	20.0	19.9	19.4
13	15.4	16.1	16.6
14	22.3	22.6	22.9
15	12.1	12.3	11.7
16	18.4	17.6	18.2
17	29.0	29.0	28.4
18	20.4	20.1	20.1
19	23.4	22.6	23.0
20	18.8	17.9	17.9
21	12.8	12.6	12.7
22	15.4	15.5	15.8
23	9.2	7.6	9.4
24	17.7	16.2	17.8
25	25.5	23.7	24.7
26	41.2	41.0	37.8
27	26.0	26.3	26.4
28	17.9	18.0	18.8
29	13.1	13.4	13.7
30	23.5	23.7	23.2
31	19.3	18.8	19.1
32	18.3	17.8	18.3
33	20.4	21.5	21.4
34	14.0	13.7	13.9
35	21.5	21.8	22.3
36	20.5	19.1	20.7

Table 3. Maximum Jet Particle Lengths (continued)

Particle	Flash No. 1 t = 295.0 (mm)	Flash No. 2 t = 375.0 (mm)	Flash No. 3 t = 470.0 (mm)
37	29.0	29.0	29.7
38	23.9	23.2	22.8
39	16.6	16.9	16.8
40	23.1	22.1	23.2
41	31.4	31.0	31.5
42	30.5	31.0	31.2
43	19.8	20.1	20.0
44	30.5	31.7	31.3
45	36.0	35.9	35.6
46	19.4	19.0	20.1
47	27.9	27.9	28.6
48	15.6	15.7	12.5
49	6.9	5.3	7.3
50	23.5	22.8	22.5
51	31.4	32.0	31.5
52	22.4	22.2	22.0
53	18.9	17.7	16.9
54	15.0	13.9	15.2
55	32.0	34.1	33.3
56	23.2	24.1	25.1
57	23.1	22.7	22.3
58	18.6	19.1	19.5
59	10.8	12.4	11.1
60	19.0	19.3	21.1
61	50.9	52.1	51.4
62	38.1	39.9	39.9

Table 4. Maximum Jet Particle Radii

Particle	Flash No. 1 t = 295.0 (mm)	Flash No. 2 t = 375.0 (mm)	Flash No. 3 t = 470.0 (mm)
1	9.53	11.33	9.82
2	2.64	3.01	2.58
3	2.08	2.26	1.86
4	2.49	4.00	2.68
5	2.95	2.57	6.08
6	2.48	2.56	2.41
7	2.22	2.27	2.53
8	2.64	2.58	2.58
9	2.90	2.69	2.41
10	2.22	—	2.24
11	2.50	2.77	2.55
12	2.57	2.47	2.48
13	2.19	2.96	2.43
14	2.57	2.98	2.57
15	2.42	2.26	2.07
16	2.70	2.82	2.74
17	2.90	2.64	2.82
18	2.78	2.90	2.81
19	3.43	2.73	2.44
20	2.62	2.58	2.50
21	2.36	2.69	2.28
22	2.75	3.14	2.81
23	2.25	2.19	2.16
24	2.38	2.08	2.20
25	2.98	2.94	2.66
26	2.86	3.20	3.07
27	2.72	2.88	2.76
28	2.47	2.85	2.52
29	2.89	2.56	2.38
30	2.51	2.65	2.52
31	2.40	2.49	2.53
32	2.46	2.54	2.37
33	2.31	2.71	2.67
34	2.37	2.67	2.47
35	2.54	2.50	2.48
36	2.66	2.83	2.60

Table 4. Maximum Jet Particle Radii (continued)

Particle	Flash No. 1 t = 295.0 (mm)	Flash No. 2 t = 375.0 (mm)	Flash No. 3 t = 470.0 (mm)
37	2.79	3.16	2.50
38	2.99	3.02	2.57
39	2.38	2.85	2.25
40	2.51	2.89	3.27
41	2.76	2.85	2.67
42	2.52	3.05	2.74
43	2.58	3.06	2.67
44	3.31	3.66	3.34
45	3.50	3.80	3.14
46	2.98	3.16	3.08
47	3.24	3.40	3.14
48	3.24	4.21	3.54
49	1.92	2.23	2.64
50	3.20	3.66	3.07
51	3.88	4.06	3.69
52	3.52	4.11	3.77
53	3.86	3.69	4.28
54	3.53	3.32	3.33
55	3.66	4.29	3.90
56	3.47	3.80	3.67
57	4.11	4.31	4.55
58	4.45	4.42	4.32
59	4.25	4.37	3.51
60	4.23	4.15	4.14
61	5.76	5.72	5.57
62	5.52	5.63	5.09

Table 5. Jet Particle Masses

Particle	Flash No. 1 t = 295.0 (g)	Flash No. 2 t = 375.0 (g)	Flash No. 3 t = 470.0 (g)
1	34.15	39.01	37.92
2	2.43	2.79	2.23
3	0.52	0.63	0.50
4	1.86	2.58	1.91
5	3.17	3.31	4.34
6	2.89	3.30	2.95
7	1.22	1.27	1.42
8	1.52	1.78	1.75
9	2.67	2.85	2.48
10	0.39	—	0.35
11	2.40	2.55	2.26
12	2.02	2.23	2.01
13	1.46	1.88	1.57
14	2.51	2.71	2.25
15	1.11	1.09	0.85
16	1.66	1.95	1.53
17	3.59	3.50	3.22
18	2.37	2.40	2.26
19	2.60	2.40	2.31
20	2.04	2.05	1.72
21	1.17	1.22	1.15
22	1.65	1.77	1.57
23	0.84	0.58	0.67
24	1.55	1.16	1.64
25	2.73	2.84	2.77
26	4.19	5.27	4.42
27	2.8[1]	3.16	2.92
28	1.59	1.98	1.77
29	1.18	1.36	1.23
30	2.46	2.55	2.40
31	1.99	2.09	1.95
32	1.65	1.86	1.73
33	1.94	2.86	2.42
34	1.20	1.50	1.29
35	1.90	2.13	1.80
36	2.21	2.55	2.32

Table 5. Jet Particle Masses (continued)

Particle	Flash No. 1 t = 295.0 (g)	Flash No. 2 t = 375.0 (g)	Flash No. 3 t = 470.0 (g)
37	3.01	3.71	3.12
38	2.80	3.36	2.60
39	1.59	2.02	1.50
40	2.33	2.82	3.38
41	3.35	4.60	3.93
42	3.14	4.62	3.76
43	1.87	2.79	2.10
44	3.82	4.63	4.21
45	5.09	6.81	5.64
46	2.15	2.59	2.35
47	4.11	4.95	4.41
48	2.24	2.65	1.89
49	0.28	0.25	0.47
50	4.08	4.80	3.54
51	4.77	5.86	4.95
52	4.01	5.04	4.36
53	3.44	3.85	3.65
54	2.66	2.94	2.56
55	6.30	8.02	6.42
56	5.39	6.40	5.63
57	5.95	6.73	6.22
58	4.63	5.29	4.74
59	2.07	2.62	1.90
60	4.65	5.05	4.94
61	25.05	26.60	22.81
62	15.03	18.39	13.85

Table 6. Summary of Individual Particle Characteristics

Particle	Length (mm)	Radius (mm)	L/D	Mass (g)	Velocity (km/s)
1	52.70	10.23	2.58	37.03	8.47
2	20.74	2.74	3.78	2.48	8.44
3	9.59	2.07	2.32	0.55	8.29
4	16.10	3.06	2.63	2.12	8.25
5	28.62	3.87	3.70	3.60	8.22
6	29.65	2.49	5.96	3.05	8.04
7	14.51	2.34	3.10	1.30	7.94
8	17.35	2.60	3.34	1.68	7.90
9	26.16	2.67	4.90	2.67	7.75
10	6.82	2.23	1.53	0.37	7.67
11	23.55	2.61	4.52	2.40	7.64
12	19.52	2.51	3.89	2.08	7.50
13	15.90	2.52	3.15	1.64	7.40
14	22.60	2.71	4.18	2.49	7.38
15	11.95	2.25	2.66	1.02	7.26
16	17.88	2.75	3.25	1.71	7.18
17	28.36	2.78	5.10	3.44	7.07
18	19.90	2.83	3.52	2.34	6.94
19	22.73	2.87	3.96	2.44	6.81
20	18.04	2.57	3.51	1.93	6.71
21	12.01	2.44	2.46	1.18	6.67
22	15.57	2.90	2.68	1.66	6.57
23	8.56	2.20	1.95	0.70	6.53
24	16.44	2.22	3.71	1.45	6.47
25	24.16	2.86	4.22	2.78	6.39
26	39.86	3.04	6.55	4.63	6.21
27	26.05	2.79	4.68	2.96	6.04
28	17.91	2.61	3.43	1.78	5.96
29	13.36	2.61	2.56	1.26	5.85
30	23.42	2.56	4.57	2.47	5.84
31	18.35	2.47	3.71	2.01	5.72
32	18.02	2.46	3.67	1.75	5.60
33	20.85	2.56	4.07	2.41	5.59
34	13.48	2.50	2.69	1.33	5.49
35	21.77	2.51	4.35	1.94	5.39
36	19.27	2.70	3.57	2.36	5.33

Table 6. Summary of Individual Particle Characteristics (continued)

Particle	Length (mm)	Radius (mm)	L/D	Mass (g)	Velocity (km/s)
37	29.22	2.82	5.18	3.28	5.22
38	23.29	2.86	4.07	2.92	5.05
39	15.93	2.49	3.20	1.70	5.02
40	22.62	2.89	3.91	2.84	4.89
41	30.55	2.76	5.53	3.96	4.78
42	30.24	2.77	5.46	3.84	4.66
43	19.58	2.77	3.53	2.26	4.51
44	31.01	3.43	4.51	4.22	4.45
45	35.81	3.48	5.15	5.85	4.27
46	18.47	3.08	3.00	2.36	4.16
47	26.26	3.26	4.02	4.49	4.04
48	14.02	3.66	1.91	2.26	3.94
49	6.48	2.26	1.43	0.34	3.88
50	21.70	3.31	3.28	4.14	3.82
51	31.48	3.88	4.06	5.19	3.69
52	20.75	3.80	2.73	4.47	3.58
53	16.91	3.95	2.14	3.65	3.45
54	14.12	3.39	2.08	2.72	3.41
55	32.23	3.95	4.08	6.92	3.29
56	23.33	3.65	3.20	5.81	3.20
57	22.21	4.32	2.57	6.30	3.05
58	18.92	4.40	2.15	4.83	2.98
59	11.09	4.04	1.37	2.20	2.90
60	17.71	4.18	2.12	4.88	2.81
61	47.69	5.69	4.19	24.82	2.78
62	37.35	5.41	3.45	15.76	2.63

Table 7. Cumulative Jet Properties

Particle	Cumulative Length (mm)	Cumulative Mass (g)	Cumulative Momentum (kg m/s)	Cumulative Energy (kJ)	Breakup Time (μs)
1	52.7	37.0	313.5	1,327.3	0.0
2	73.4	39.5	334.5	1,415.8	1,210.7
3	83.0	40.1	339.1	1,434.7	296.0
4	99.1	42.2	356.5	1,506.8	302.4
5	127.8	45.8	386.1	1,628.5	347.7
6	157.4	48.8	410.7	1,727.0	270.4
7	171.9	50.1	421.0	1,768.1	262.5
8	189.3	51.8	434.3	1,820.6	270.0
9	215.4	54.5	455.0	1,900.6	244.2
10	222.2	54.9	457.8	1,911.5	241.5
11	245.8	57.3	476.2	1,981.7	251.8
12	265.3	59.3	491.8	2,040.3	237.4
13	281.2	61.0	503.9	2,085.2	231.9
14	303.8	63.5	522.3	2,153.0	244.3
15	315.8	64.5	529.7	2,179.8	235.3
16	333.6	66.2	542.0	2,224.0	232.0
17	362.0	69.6	566.3	2,309.9	230.2
18	381.9	72.0	582.5	2,366.3	225.8
19	404.6	74.4	599.1	2,422.7	220.8
20	422.7	76.4	612.1	2,466.2	220.6
21	434.7	77.5	620.0	2,492.5	223.4
22	450.3	79.2	630.9	2,528.3	218.8
23	458.8	79.9	635.4	2,543.2	220.6
24	475.3	81.4	644.9	2,573.6	221.0
25	499.4	84.1	662.6	2,630.5	222.4
26	539.3	88.8	691.4	2,719.8	218.6
27	565.3	91.7	709.3	2,773.8	216.7
28	583.2	93.5	719.9	2,805.5	218.7
29	596.6	94.8	727.3	2,827.0	215.2
30	620.0	97.2	741.7	2,869.1	221.7
31	638.4	99.2	753.2	2,902.0	219.7
32	656.4	101.0	763.0	2,929.4	216.3
33	677.2	103.4	776.4	2,966.9	222.3
34	690.7	104.7	783.7	2,987.1	221.2
35	712.5	106.7	794.2	3,015.3	219.8

Table 7. Cumulative Jet Properties (continued)

Particle	Cumulative Length (mm)	Cumulative Mass (g)	Cumulative Momentum (kg m/s)	Cumulative Energy (kJ)	Breakup Time (μs)
36	731.8	109.0	806.8	3,048.9	222.1
37	761.0	112.3	823.9	3,093.6	222.0
38	784.3	115.2	838.7	3,130.9	218.6
39	800.2	116.9	847.2	3,152.3	222.0
40	822.8	119.8	861.1	3,186.4	219.7
41	853.4	123.7	880.0	3,231.5	219.9
42	883.6	127.6	898.0	3,273.3	221.4
43	903.2	129.8	908.1	3,296.3	219.2
44	934.2	134.0	926.9	3,338.1	222.1
45	970.0	139.9	951.9	3,391.3	220.5
46	988.5	142.3	961.7	3,411.8	221.2
47	1,014.7	146.7	979.8	3,448.3	220.1
48	1,028.8	149.0	988.7	3,465.9	220.1
49	1,035.2	149.3	990.0	3,468.4	219.3
50	1,056.9	153.5	1,005.8	3,498.6	219.2
51	1,088.4	158.7	1,025.0	3,534.0	219.2
52	1,109.2	163.1	1,041.0	3,562.7	219.6
53	1,126.1	166.8	1,053.6	3,584.5	217.7
54	1,140.2	169.5	1,062.9	3,600.3	218.9
55	1,172.4	176.4	1,085.7	3,637.8	218.4
56	1,195.8	182.2	1,104.3	3,667.5	219.8
57	1,218.0	188.5	1,123.5	3,696.8	217.8
58	1,236.9	193.4	1,138.0	3,718.4	218.7
59	1,248.0	195.6	1,144.4	3,727.7	218.5
60	1,265.7	200.5	1,158.1	3,747.0	217.7
61	1,313.4	225.3	1,227.1	3,842.8	222.0
62	1,350.7	241.1	1,268.5	3,897.1	223.6

	With Tip	Without Tip
Average Length (mm)	21.79	21.28
Average Radius (mm)	3.14	3.02
Average L/D	3.529	3.544
Average Velocity Change (km/s)	0.096	0.097

Table 8. Drift Velocity Measurements

Particle	Axial Velocity (km/s)	Drift Velocity (m/s)	Dispersion Angle (°)
1	8.467	13.242	225.739
2	8.437	11.400	30.913
3	8.292	11.252	29.515
4	8.253	7.779	36.841
5	8.217	9.499	36.026
6	8.037	3.506	38.910
7	7.940	3.915	36.142
8	7.896	5.193	36.865
9	7.747	6.037	34.568
10	7.670	58.189	18.808
11	7.642	12.185	32.026
12	7.502	14.518	31.152
13	7.402	11.888	26.035
14	7.378	15.724	30.273
15	7.262	15.159	31.956
16	7.181	15.940	27.574
17	7.071	19.854	26.537
18	6.936	21.287	29.631
19	6.806	25.394	27.871
20	6.712	24.927	25.638
21	6.666	20.469	25.301
22	6.565	32.204	29.134
23	6.526	18.434	23.000
24	6.473	12.076	32.066
25	6.394	5.110	41.954
26	6.212	3.132	81.510
27	6.040	4.017	122.983
28	5.962	5.089	173.968
29	5.848	5.609	162.137
30	5.842	6.684	178.426
31	5.723	8.975	181.381
32	5.596	12.964	210.551
33	5.586	11.046	196.388
34	5.494	11.736	200.742
35	5.395	12.706	205.695

Table 8. Drift Velocity Measurements (continued)

Particle	Axial Velocity (km/s)	Drift Velocity (m/s)	Dispersion Angle (°)
36	5.334	10.522	194.971
37	5.224	8.215	181.061
38	5.054	8.362	188.385
39	5.017	11.865	210.335
40	4.894	9.151	202.505
41	4.775	7.573	200.199
42	4.664	8.206	208.554
43	4.512	8.655	212.638
44	4.449	7.118	212.141
45	4.269	2.737	151.212
46	4.159	2.684	132.269
47	4.037	2.938	115.219
48	3.944	3.577	115.163
49	3.882	8.019	96.817
50	3.815	4.102	200.109
51	3.694	4.491	93.243
52	3.583	4.792	205.258
53	3.455	5.047	123.651
54	3.412	8.128	105.527
55	3.293	4.607	138.745
56	3.200	9.230	224.767
57	3.048	13.738	253.881
58	2.977	11.314	252.757
59	2.903	12.924	248.924
60	2.814	12.923	274.638
61	2.778	10.343	224.817
62	2.627	11.550	226.318

5. REFERENCES

Blische, H. J., and B. M. Simmons. "A Method for Reducing Data from Radiographs of Shaped-Charge Jets." BRL-TR-02330, U.S. Army Ballistic Research Laboratory, Aberdeen Proving Ground, MD, June 1981.

Held, M. "Determination of the Material Quality of Copper Shaped Charge Liners." Propellants, Explosives, Pyrotechnics, vol. 10, pp. 125–128, 1985.

Held, M. "Particulation of Shaped Charge Jets." Proceedings of the 11th International Symposium on Ballistics, Brussels, May 1989.

Held, M., and P. Nikowitsch. "Comparative Investigation of Flash X-Ray Pictures and SST-Records for Diagnostic Evaluation of Shaped Charge Jets." Proceedings of the 16th International Symposium on High Speed Photography and Photonics, Strasbourg, SPIE vol. 491, pp. 614–618, 1984.

Fenton, G. K., and D. J. Butz. "Semi-Automated Analysis of Shaped Charge Jets." 1989 Flash Radiography Topical Symposium, Welches, OR, 14–18 August 1989.

Lystad, H. A., et al. "Automated Data Reduction from Flash X-Radiographs of Jets from Lined Shaped Charges." 1989 Flash Radiography Topical Symposium, pp. 152–159, Welches, OR, 14–18 August 1989.

Segletes, S. "Drift Velocity Computations for Shaped-Charge Jets." ARBRL-MR-03306, U.S. Army Ballistic Research Laboratory, Aberdeen Proving Ground, MD, September 1983.

Segletes, S. "Improved Drift Velocity Computations for Shaped-Charge Jets." BRL-TR-2823, U.S. Army Ballistic Research Laboratory, Aberdeen Proving Ground, MD, June 1987.

Sewell, D. "The Measurement of the Lateral Velocities of Shaped Charge Jets Using Flash Radiography." Proceedings of the 1989 Flash Radiography Topical Symposium, pp. 296–305, Welches, OR, 14–18 August 1989.

Simon, J. "The Effect of Explosive Detonation Characteristics on Shaped Charge Performance." BRL-MR-2414, U.S. Army Ballistic Research Laboratory, Aberdeen Proving Ground, MD, 1974.

Summers, R. L., and K. C. Wright. "The Experimental Assessment of Jet Transverse Velocity." Developments in Theoretical and Applied Mechanics, vol. XVI, pp. II.8.17–II.8.24, University of Tennessee Space Institute, Tullahoma, TN, April 1992.

Summers, R. L., W. P. Walters, and R. D. Dick. "The Behavior of Shaped Charges with Open-Poled Hemispherical Liners." BRL-TR-3169, U.S. Army Ballistic Research Laboratory, Aberdeen Proving Ground, November 1990.

Verhagen Th. L. A., and J. L. M. J. Van Bree. "Digital Image Processing Applied to Flash X-Ray Shadowgraphs to Determine Fragment Mass Distribution." Proceedings of the 10th International Symposium on Ballistics, San Diego, CA, October 1987.

Verhagen, Th. L. A., and J. L. M. J. Van Bree. "Reconstruction of Fragment Mass Distribution from Flash Radiographs." 1989 Flash Radiography Topical Symposium, pp. 355–364, Welches, OR, 14–18 August 1989.

Van Bree, J. L. M. J., and Th. L. A. Verhagen. "Determination of Fragment Mass Distributions From Flash X-Ray Shadowgraphs With Digital Image Processing." Proceedings of the 37th Aeroballistic Range Association, Quebec, Canada, 1986.

No. of Copies	Organization
2	Administrator Defense Technical Info Center ATTN: DTIC-DDA Cameron Station Alexandria, VA 22304-6145
1	Commander U.S. Army Materiel Command ATTN: AMCAM 5001 Eisenhower Ave. Alexandria, VA 22333-0001
1	Commander U.S. Army Laboratory Command ATTN: AMSLC-DL 2800 Powder Mill Rd. Adelphi, MD 20783-1145
2	Commander U.S. Army Armament Research, Development, and Engineering Center ATTN: SMCAR-IMI-I Picatinny Arsenal, NJ 07806-5000
2	Commander U.S. Army Armament Research, Development, and Engineering Center ATTN: SMCAR-TDC Picatinny Arsenal, NJ 07806-5000
1	Director Benet Weapons Laboratory U.S. Army Armament Research, Development, and Engineering Center ATTN: SMCAR-CCB-TL Watervliet, NY 12189-4050
(Unclass. only)1	Commander U.S. Army Rock Island Arsenal ATTN: SMCRI-TL/Technical Library Rock Island, IL 61299-5000
1	Director U.S. Army Aviation Research and Technology Activity ATTN: SAVRT-R (Library) M/S 219-3 Ames Research Center Moffett Field, CA 94035-1000
1	Commander U.S. Army Missile Command ATTN: AMSMI-RD-CS-R (DOC) Redstone Arsenal, AL 35898-5010

No. of Copies	Organization
1	Commander U.S. Army Tank-Automotive Command ATTN: ASQNC-TAC-DIT (Technical Information Center) Warren, MI 48397-5000
1	Director U.S. Army TRADOC Analysis Command ATTN: ATRC-WSR White Sands Missile Range, NM 88002-5502
1	Commandant U.S. Army Field Artillery School ATTN: ATSF-CSI Ft. Sill, OK 73503-5000
(Class. only)1	Commandant U.S. Army Infantry School ATTN: ATSH-CD (Security Mgr.) Fort Benning, GA 31905-5660
(Unclass. only)1	Commandant U.S. Army Infantry School ATTN: ATSH-CD-CSO-OR Fort Benning, GA 31905-5660
1	WL/MNOI Eglin AFB, FL 32542-5000
	Aberdeen Proving Ground
2	Dir, USAMSAA ATTN: AMXSY-D AMXSY-MP, H. Cohen
1	Cdr, USATECOM ATTN: AMSTE-TC
3	Cdr, CRDEC, AMCCOM ATTN: SMCCR-RSP-A SMCCR-MU SMCCR-MSI
1	Dir, VLAMO ATTN: AMSLC-VL-D
10	Dir, USABRL ATTN: SLCBR-DD-T

No. of
Copies Organization

4 Commander
Naval Surface Warfare Center
ATTN: Code DG-50,
W. Reed, R10A
E. Johnson
W. Bullock
Code DX-21, Lib Br
White Oak, MD 20910

2 Commander
U.S. Army Armament Research,
Development, and Engineering Center
ATTN: SMCAR-AWE,
J. Pearson
J. Grant
Picatinny Arsenal, NJ 07806-5000

3 Director
Defense Advanced Research Projects
Agency
ATTN: J. Richardson
LTC Quinn
T. Hafer
3701 North Fairfax Dr.
Arlington, VA 22203-1714

5 Commander
U.S. Army Missile Command
ATTN: AMSMI-RD-ST-WF,
M. Schexnayder
S. Cornelius
D. Lovelace
A. McDonald
S. Hill
Redstone Arsenal, AL 35898-5247

1 AFATL/DLJR (J. Foster)
Eglin AFB, FL 32542

1 WRDC/MTX (Lee Kennard)
Wright-Patterson AFB, OH 45443-6533

1 Director
U.S. Army Harry Diamond Laboratories
ATTN: SLCHD-TA-SS, Bob Christopherson
2800 Powder Mill Road
Adelphi, MD 20783-1197

No. of
Copies Organization

1 Director
Lawrence Livermore National Laboratory
ATTN: Technical Library
P.O. Box 808
Livermore, CA 94550

2 Battelle
ATTN: TACTEC Library, J. N. Huggins
Dr. L. Vescilius
505 King Avenue
Columbus, OH 43201

3 Director
Sandia National Laboratories
ATTN: Dr. M. Forrestal
Dr. M. Vigil
Dr. A. Robinson
P.O. Box 5800
Albuquerque, NM 87185

7 University of California
Los Alamos Scientific Laboratory
ATTN: Dr. J. Walsh
Dr. R. Karpp
Dr. C. Mautz
L. Hull, M-8
J. Repa
D. Fradkin
Technical Library
P.O. Box 1663
Los Alamos, NM 87545

1 Battelle
Edgewood Operations
ATTN: R. Jameson
2113 Emmorton Park Road
Suite 200
Edgewood, MD 21040

1 E.I. DuPont De Nemours & Company
ATTN: B. Scott
Chestnut Run - CR 702
Wilmington, DE 19898

1 Dyna East Corporation
ATTN: P. C. Chou
3201 Arch Street
Philadelphia, PA 19104-2588

No. of
Copies Organization

1 Aerojet General Corporation
ATTN: Warhead Systems, Dr. J. Carleone
P.O. Box 296
Azusa, CA 91702

INTENTIONALLY LEFT BLANK.

USER EVALUATION SHEET/CHANGE OF ADDRESS

This Laboratory undertakes a continuing effort to improve the quality of the reports it publishes. Your comments/answers to the items/questions below will aid us in our efforts.

1. BRL Report Number BRL-TR3393 Date of Report September 1992

2. Date Report Received _____

3. Does this report satisfy a need? (Comment on purpose, related project, or other area of interest for which the report will be used.) _____

4. Specifically, how is the report being used? (Information source, design data, procedure, source of ideas, etc.) _____

5. Has the information in this report led to any quantitative savings as far as man-hours or dollars saved, operating costs avoided, or efficiencies achieved, etc? If so, please elaborate. _____

6. General Comments. What do you think should be changed to improve future reports? (Indicate changes to organization, technical content, format, etc.) _____

CURRENT ADDRESS

Name

Organization

Address

City, State, Zip Code

7. If indicating a Change of Address or Address Correction, please provide the New or Correct Address in Block 6 above and the Old or Incorrect address below.

OLD ADDRESS

Name

Organization

Address

City, State, Zip Code

(Remove this sheet, fold as indicated, staple or tape closed, and mail.)

DEPARTMENT OF THE ARMY
Director
U.S. Army Ballistic Research Laboratory
ATTN: SLCBR-DD-T
Aberdeen Proving Ground, MD 21005-5066

OFFICIAL BUSINESS

BUSINESS REPLY MAIL
FIRST CLASS PERMIT No 0001, APG, MD

Postage will be paid by addressee.

Director
U.S. Army Ballistic Research Laboratory
ATTN: SLCBR-DD-T
Aberdeen Proving Ground, MD 21005-5066

NO POSTAGE
NECESSARY
IF MAILED
IN THE
UNITED STATES